Effects of Bacterial Density on Growth Rate and Characteristics of Microbial-Induced $CaCO_3$ Precipitates: Particle-Scale Experimental Study

Yuze Wang, Ph.D., M.ASCE[1]; Kenichi Soga, Ph.D., F.ASCE[2]; Jason T. DeJong, Ph.D., F.ASCE[3]; and Alexandre J. Kabla, Ph.D.[4]

Abstract: Microbial-induced carbonate precipitation (MICP) has been explored for more than a decade as a promising soil improvement technique. However, it is still challenging to predict and control the growth rate and characteristics of $CaCO_3$ precipitates, which directly affect the engineering performance of MICP-treated soils. In this study, we employ a microfluidics-based pore-scale model to observe the effect of bacterial density on the growth rate and characteristics of $CaCO_3$ precipitates during MICP processes occurring at the sand particle scale. Results show that the precipitation rate of $CaCO_3$ increases with bacterial density in the range between 0.6×10^8 and 5.2×10^8 cells/mL. Bacterial density also affects both the size and number of $CaCO_3$ crystals. A low bacterial density of 0.6×10^8 cells/mL produced 1.1×10^6 crystals/mL with an average crystal volume of 8,000 μm^3, whereas a high bacterial density of 5.2×10^8 cells/mL resulted in more crystals (2.0×10^7 crystals/mL), but with a smaller average crystal volume of 450 μm^3. The produced $CaCO_3$ crystals were stable when the bacterial density was 0.6×10^8 cells/mL. When the bacterial density was 4–10 times higher, the crystals were first unstable and then transformed into more stable $CaCO_3$ crystals. This suggests that bacterial density should be an important consideration in the design of MICP protocols.
DOI: 10.1061/(ASCE)GT.1943-5606.0002509.

Author keywords: Soil stabilization; Ground improvement; Particle-scale behavior; Microscopy; Time dependence; Mineralogy; Microbial-induced $CaCO_3$ precipitation.

Introduction

Microbial-induced calcium carbonate precipitation (MICP) has been extensively investigated for applications such as ground improvement, soil liquefaction mitigation, dam safety control, prevention of soil erosion, and slope stabilization (Van Paassen 2009; DeJong et al. 2013; Martinez et al. 2013; Montoya et al. 2013; Jiang et al. 2017). The $CaCO_3$ precipitates fill soil pores and bond soil particles, which consequently increase the strength and stiffness, and reduce the permeability of the soil matrix (Stocks-Fischer et al. 1999; DeJong et al. 2006). Several types of bacterial activities including ureolysis, denitrification, and sulfate reduction can result in MICP (DeJong et al. 2010), and among those, the ureolysis-based process has been most widely studied. Ureolysis-driven MICP involves urea hydrolysis by the urease enzyme produced by active microorganisms [Eq. (1)], resulting in the generation of calcium carbonate ($CaCO_3$) in the soil matrix [Eq. (2)]

$$CO(NH_2)_2 + 2H_2O \xrightarrow{Urease} 2NH_4^+ + CO_3^{2-} \quad (1)$$

$$Ca^{2+} + CO_3^{2-} \rightarrow CaCO_3(s) \quad (2)$$

Ureolysis and $CaCO_3$ precipitation are the two key processes involved in the ureolysis-driven MICP process. Understanding the kinetics of these two processes is essential for designing MICP protocols. The kinetics of ureolysis is normally assessed by the increase in solution conductivity due to the hydrolysis of urea (Whiffin et al. 2007; Lauchnor et al. 2015). The kinetics of $CaCO_3$ precipitation can be assessed by the decrease in Ca^{2+} concentration (Stocks-Fischer et al. 1999). Recently, the kinetics of $CaCO_3$ at the crystal size level have also been studied by using optical microscopes to observe $CaCO_3$ crystals produced in liquid medium in Petri dishes (Zhang et al. 2018), on glass slides (Wang et al. 2019b), or in microfluidic chips (Wang et al. 2017, 2019a, b; Kim et al. 2020), as well as in crystals produced on solid agar pads (Zhang et al. 2018). Crystals grew steadily to diameters of 20 and 50 μm within 40 min when MICP occurred in a liquid medium placed in a Petri dish or on an agar pad containing Ca^{2+} urea, respectively (Zhang et al. 2018). In comparison, the use of a microfluidic-based porous model is considered to be a more appropriate approach to study the kinetics of MICP, as it more closely mimics real MICP conditions occurring in the pore fluid of a porous soil matrix where bacterial cells move freely and the cementation solution can be injected multiple times (Wang et al. 2019a, b).

In addition to the $CaCO_3$ precipitation kinetics, the properties of $CaCO_3$ precipitates also need to be considered in a MICP protocol design. Larger crystals that bond soil particles more sufficiently may

[1]Assistant Professor, Dept. of Ocean Science and Engineering, Southern Univ. of Science and Technology, Shenzhen 518055, People's Republic of China; Southern Marine Science and Engineering Guangdong Laboratory (Guangzhou), Shenzhen 518055, People's Republic of China (corresponding author). ORCID: https://orcid.org/0000-0003-3085-5299. Email: wangyz@sustech.edu.cn

[2]Chancellor's Professor, Dept. of Civil and Environmental Engineering, Univ. of California, Berkeley, Berkeley, CA 94720. Email: soga@berkeley.edu

[3]Professor, Dept. of Civil and Environmental Engineering, Univ. of California, Davis, Davis, CA 95616. ORCID: https://orcid.org/0000-0002-9809-955X. Email: jdejong@ucdavis.edu

[4]Reader, Dept. of Engineering, Univ. of Cambridge, Cambridge CB21PZ, UK. Email: ajk61@cam.ac.uk

Note. This manuscript was submitted on July 1, 2020; approved on January 8, 2021; published online on April 9, 2021. Discussion period open until September 9, 2021; separate discussions must be submitted for individual papers. This paper is part of the ***Journal of Geotechnical and Geoenvironmental Engineering***, © ASCE, ISSN 1090-0241.

increase soil strength more effectively (Cheng et al. 2017). By conducting soil column experiments and by using scanning electron microscopy to scan the samples after MICP treatment, it was found that the concentration of cementation solution and ureolysis activity affected the size and number of $CaCO_3$ crystals after MICP treatment (Al Qabany and Soga 2013; Cheng et al. 2017). Al Qabany and Soga (2013) found that when the total treatment duration and the total amount of cementation solution were constant, the use of higher concentrations of cementation solution produced larger $CaCO_3$ crystals. Cheng et al. (2017) showed that higher bacterial activities tend to produce smaller $CaCO_3$ crystals at the end of MICP treatment.

Because $CaCO_3$ crystals were only observed after MICP treatment by using scanning electron microscopy (Al Qabany and Soga 2013; Cheng et al. 2017), the kinetics and characteristics of microbial-induced $CaCO_3$ precipitation were not fully understood. Wang et al. (2019a) designed and fabricated a microfluidic chip etched with porous models and used it to observe the MICP process under conditions that resemble soil assemblies. The advantage of this method is that the density of bacteria and the main parameters of $CaCO_3$ crystals such as size, shape, and number can be quantified during the whole MICP process (Wang et al. 2019a, b). Wang et al. (2019b) found that when the bacterial activity and concentration of cementation solution were kept constant, longer injection intervals (23–25 h compared to 3–5 h) produced larger and fewer $CaCO_3$ crystals. This was because when the interval was longer, the smaller and less stable crystals dissolved while the larger and more stable crystals continued to grow (Wang et al. 2019b).

Therefore, to gain a better understanding of the kinetics and properties of MICP, it is essential to investigate the processes of MICP rather than only the MICP properties after MICP treatment to have a better understanding of the kinetics and properties of MICP. Due to the fact that bacterial density has a direct effect on ureolysis activity (Lauchnor et al. 2015) and a large range of bacterial densities have been used in MICP studies (Al Qabany et al. 2012; Cheng et al. 2017), it is essential to know the quantity and activity of the bacteria injected into the soil to design robust MICP treatment protocols. In this study, microfluidic experiments were conducted to observe both the growth kinetics and characteristics of microbial-induced $CaCO_3$ crystals under conditions where the bacterial densities varied. The test results were used to investigate the effects of bacterial density on the kinetics and characteristics of $CaCO_3$ precipitation and to provide suggestions for MICP treatment protocols.

Materials and Methods

Microfluidic Chip Experimental Setup and Data Acquisition

The microfluidic chip used in this study was designed based on a cross-sectional image of a solidified and sectioned 3D Ottawa 30–50 sandy soil specimen and the fabrication of the microfluidic chip was conducted following the standard photolithography techniques by using polydimethylsiloxane (PDMS) and glass. The design and fabrication methods of the microfluidic chips were discussed in Wang et al. (2019a). The experimental setup is shown in Fig. 1.

During the experiments, all images were acquired with an Axio Observer Z1 research microscope (Zeiss, Cambourne, Cambridge, UK). The microscope is a phase-contrast microscope and is equipped with an automated stage (Prior Scientific Instrument, Cambridge, UK), a grayscale camera (Hamamatsu C11440-22CU, Hamamatsu, Welwyn Garden City, Hertfordshire, UK), and a light source connected to a computer and controlled by Zeiss AxioVision image analysis software. Images were captured using phase-field illumination and 10× inverted objectives (with image resolutions of 0.65 μm/pixel). Under the phase-contract microscope, bacterial cells appeared as black dots, the $CaCO_3$ precipitates appeared as white dots, and the microfluidic chip appeared as a light-to-dark grey background (Wang et al. 2019b).

Preparation of Bacterial Suspension and Cementation Solution

Sporosarcina pasteurii (DSM 33) (Leibniz Institute DSMZ-German Collection of Microorganisms and Cell Cultures GmbH, Braunschweig, Germany), a ureolytic bacterial strain, was used in the experiments. Bacterial cells from the glycerol stock (Wang et al. 2019b) were grown in ATCC 1376 NH_4-YE agar medium (20 g/L yeast extract, 10 g/L ammonium sulfate, 20 g/L

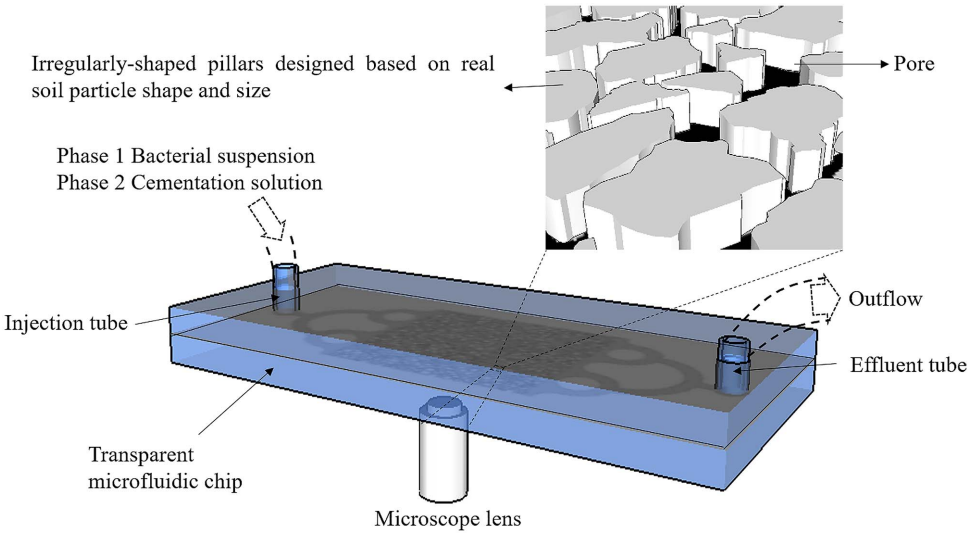

Fig. 1. Schematic of the microfluidic chip experiments. [Republished with permission of ICE Publishing, from "A microfluidic chip and its use in characterizing the particle-scale behaviour of Microbial-Induced Carbonate Precipitation (MICP)," Y. Wang, K. Soga, J. T. Dejong, A. J. Kabla, *Géotechnique*, Vol. 69 (12), pp. 1086–1094, © 2019; permission conveyed through Copyright Clearance Center, Inc.]

J. Geotech. Geoenviron. Eng., 2021, 147(6): 04021036

Table 1. Summary of bacterial, chemical, and injection parameters associated with the microfluidic chip experiments

Condition No.	Dilution ratio	Bacterial OD_{600}	Injection number	Injection interval (day)
1	1:14	0.2	12	1
2	1:5	0.5	1	—
3	1:2	1.0	12	1
4	2:1	2.0	1	—
5	1:0	3.0	12	1

agar, and 0.13 M Tris base) for 48 h at 30°C. Subsequently, several colonies on the agar plate were transferred to an NH_4-YE liquid medium containing the same components without agar and cultivated in a shaking incubator for 24 h at 30°C and at a shaking rate of 200 rotations per minute (rpm) to obtain a bacterial suspension with an optical density measured at a wavelength of 600 nm (OD_{600}) of around 3.0. A more detailed description of the preparation of the bacterial suspension can be found in Wang et al. (2019b). The cementation solution contained 0.25 mol/L of $CaCl_2$, 0.375 mol/L of urea, and 3 g/L of nutrient broth.

Staged Injection Procedure of Cementation Solution to Produce $CaCO_3$ Precipitates

A staged injection procedure was applied to the MICP treatment process. After bacterial injection into a microfluidic chip and the subsequent 2-h bacterial settling period, 1.25 pore volumes (PV) of cementation solution were injected into the microfluidic chip at an injection flow rate of 5.6 PV/h. Subsequent injections of cementation solution were conducted at 24-h intervals after the previous injection. In total, 12 injections of cementations solution were applied. The injection volume of the cementation solution, the flow rate, and the number of injections of cementation solution were chosen based on findings presented in Wang et al. (2019a, b). Time-series images were captured at 15 min intervals after the completion of each of the cementation solution injections. The main experimental parameters in these protocols are summarized in Table 1.

Quantification of Bacterial Density and Activity

Bacterial suspensions with five different densities were prepared to correlate with bacterial optical density. The OD_{600} was measured to quantify the bacterial density before the injection of 1.5 PV into each of five microfluidic chips at an injection flow rate of 56 PV/h. The bacterial suspensions were prepared by diluting the bacterial suspension with OD_{600} of 3.0 using autoclaved NH_4-YE liquid medium at volume proportions V_bacterial suspension: V_NH_4-YE liquid medium of 1:14, 1:5, 1:2, 2:1, and 1:0. NH_4-YE liquid medium provides nutrients for bacterial activity. Therefore, to avoid bacterial starvation, autoclaved NH_4-YE liquid medium instead of deionized water was used to dilute the bacterial suspension from OD_{600} of 3.0 to prepare bacterial suspensions at lower densities. It should be noted that due to the difference in dilution ratios, the amount of nutrients provided to the bacterial cells varies when the bacterial densities are different, and this difference was not considered in this study. Injecting 1.5 PV of a bacterial suspension at a flow rate of 56 PV/h resulted in a homogeneous distribution of bacteria after injection (Wang et al. 2019a). The bacterial density was quantified based on the images taken at the center of the microfluidic chips. Bacteria were given 10 min to settle to the bottom zone of the microfluidic chip before obtaining accurate microscope images since the microscope focal length depth range was 17 μm, whereas the depth of the microfluidic chip was 50 μm. The bacterial cells doubled in number in about 2 h due to *in situ* growth during bacterial settling (Wang et al. 2019a). The effect of bacterial growth on the bacterial density changed during the first 10 min, but this was neglected due to the short period. Because bacterial size affects the reading of OD_{600} value (Zapata and Ramirez-Arcos 2015), the sizes of the bacteria were also measured to obtain the average bacterial size.

To examine the effect of bacterial density on the rate of ureolysis, a series of batch tests were conducted by varying the bacterial densities in bacteria-urea mixtures. The hydrolysis rate was measured using the conductivity method described by Whiffin et al. (2007). The urea concentration in the bacteria-urea mixtures was 1.0 M before the hydrolysis of urea occurred. The bacterial densities in the bacteria-urea mixtures were equivalent to OD_{600} of 0.1, 0.25, 0.46, 0.75, 1.035, 1.38, and 1.73. The conductivity of the mixed content was assessed by using a conductivity meter (FiveGo, Mettler-Toledo, Beaumont Leys, Leicester, UK) immediately after the mixing and 5 min after mixing. The ureolysis rate was calculated using Eq. (3) (Whiffin et al. 2007). Measurements were performed in triplicate for each of the different media tested, with data presented as mean ± standard error

$$Ureolysis\ rate(\mathrm{mM/h}) = \frac{\Delta Conductivity(\mu\mathrm{S/cm})}{\Delta t(\mathrm{min})} \times (10^{-3} \times 11.11)(\mathrm{mM}/(\mu\mathrm{S/cm})) \times 60(\mathrm{min/h}) \quad (3)$$

Quantification of Crystal Growth Rate, Size, and Quantity

Several methods were used to quantify $CaCO_3$ crystal characteristics. The mean intensity values of the images were analyzed using Zeiss Axio Vision image analysis software and plotted against time to show how the relative areas occupied by the precipitates changed with time. The image intensities could not represent the total crystal volume produced because two-dimensional images cannot capture the entire information of the three-dimensional crystals, but could represent the change in crystal properties with time. In addition, crystal diameter has previously been used to quantify the size of $CaCO_3$ crystals (Zhang et al. 2018). During the initial growth stage, most crystals were hemispheres and grew on the surface of the microfluidic channel (Wang et al. 2019; Kim et al. 2020). Therefore, in this study, the volumes of individual crystals were calculated based on their measured diameters. In addition, the number of crystals was also counted.

Results and Discussion

Bacterial Density and Bacterial Optical Density

The bacterial densities of five bacterial suspensions (cells/mL) were correlated with their initial OD_{600} values to quantify the bacterial density used. Microscope images were taken at the center of five microfluidic chips containing bacterial suspensions with the initial OD_{600} of 0.2, 0.5, 1.0, 2.0, and 3.0 at 10 min after the injection of bacterial suspensions [shown in Fig. 2(a)]. Bacterial densities correlated with the initial OD_{600} values of the bacterial suspensions, and the results are shown in Fig. 2(b). A blank sample with no bacterial cells in the bacterial nutrient liquid was used as a baseline against which the OD_{600} was defined as zero. The data show that bacterial density and OD_{600} are linearly correlated as

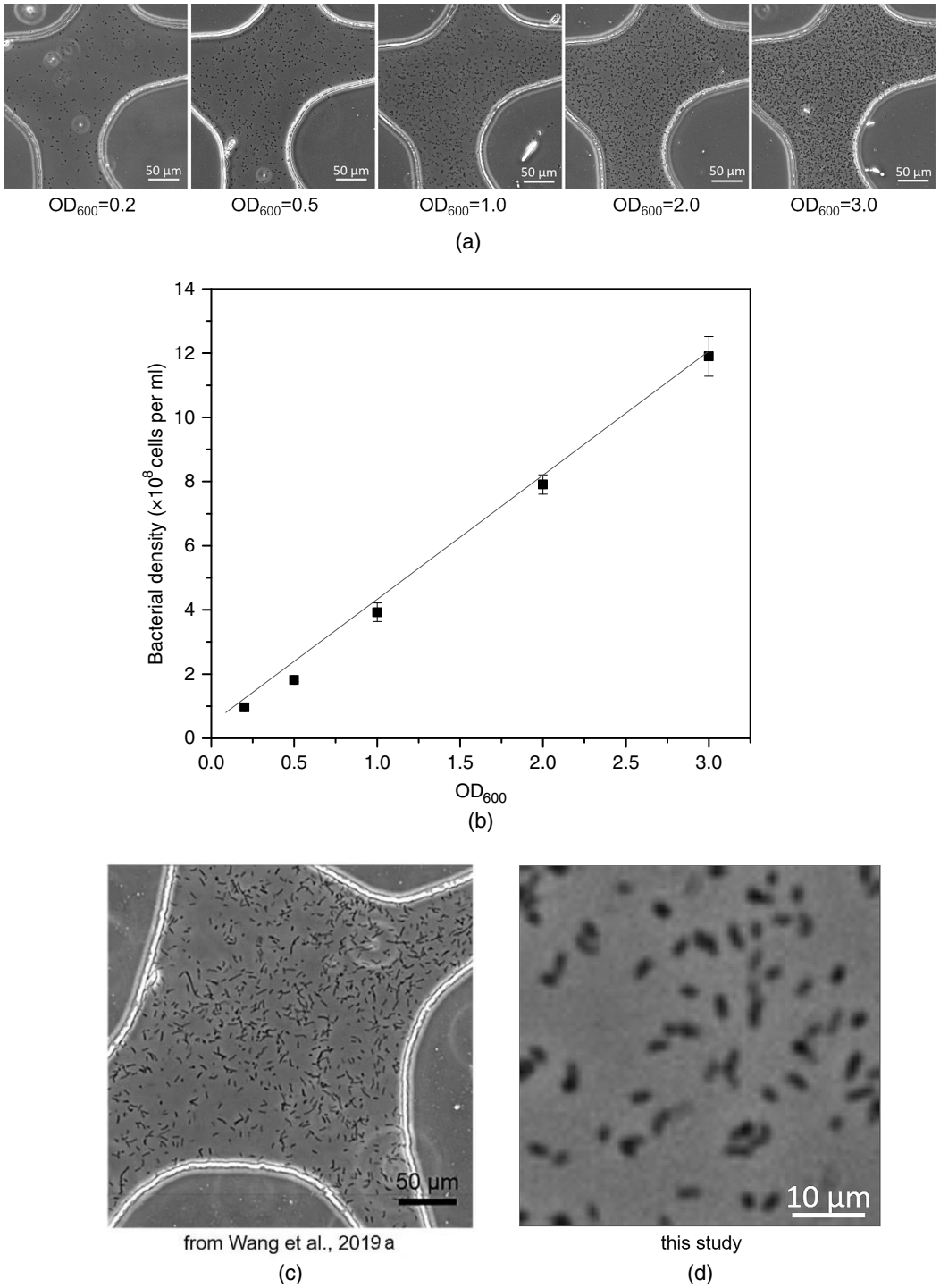

Fig. 2. (a) Microscope images of one pore at the center of the microfluidic chip taken at 10 min after the injection of bacterial suspensions with initial OD_{600} values of 0.2, 0.5, 1.0, 2.0, and 3.0; (b) correlations between the initial OD_{600} of the bacterial suspensions and bacterial density at 10 min after bacterial injection, cell concentration $= OD_{600} \times 4 \times 10^8$, data are presented as mean $\pm$ standard error, and each measurement was repeated three times; and (c) image of one pore at the center of the microfluidic chip taken at 2 h after the injection of a bacterial suspension with initial OD_{600} values of 0.8 showing bacteria with a size of approximately 10 μm [Republished with permission of ICE Publishing, from "A microfluidic chip and its use in characterizing the particle-scale behaviour of Microbial-Induced Carbonate Precipitation (MICP)," Y. Wang, K. Soga, J. T. Dejong, A. J. Kabla, *Géotechnique*, Vol. 69 (12), pp. 1086–1094, © 2019; permission conveyed through Copyright Clearance Center, Inc.]; and (d) magnified image of middle image of (a) showing bacterial size being about 3 μm in this study.

$$Bacterial\ density(\text{cells/mL}) = OD_{600} \times 4 \times 10^8 \qquad (4)$$

The R^2 value of the regression line in Fig. 2(b) is higher than 0.99.

Because bacterial cell size affects the optical density of a bacterial suspension, magnified images of the microfluidic chips containing bacterial suspensions in this study and a previous study (Wang et al. 2019a) are presented to show how the difference in bacterial

cell size would affect the optical density of the bacterial suspension [Figs. 2(c and d)]. The sizes of bacterial cells in this study are about 3 μm, whereas those in Wang et al. (2019a) are about 10 μm. Consequently, at the same optical density, the bacterial density in this study is about 3 times higher than that in Wang et al. (2019a). Because of the difference in bacterial size, the ureolysis rate may vary when the bacterial optical densities are the same. Therefore, in this study, the bacterial cells were obtained from one batch of bacterial suspension, where the sizes of bacterial cells were relatively consistent, and the bacterial densities were modified to obtain a variety of bacterial activities in terms of ureolysis rate.

Bacterial Density During MICP Processes

Three MICP processes using different bacterial densities were conducted in microfluidic experiments. Optical densities of the bacterial suspensions were measured prior to the injections of bacterial suspensions. Bacterial densities (in cells per mL) of the bacterial suspensions were quantified (1) after injection of bacterial suspension, (2) after 2 h of settling, and (3) after injection of the cementation solution. The results are presented in Table 2. The corresponding microscope images and results are presented in Figs. 3(a and b), respectively. When the initial bacterial densities were $(0.96 \pm 0.03) \times 10^8$, $(3.92 \pm 0.29) \times 10^8$, and $(11.90 \pm 0.61) \times 10^8$ cells/mL; after 2 h of settling, the bacterial densities increased to $(1.92 \pm 0.13) \times 10^8$, $(6.09 \pm 0.34) \times 10^8$, and $(15.4 \pm 0.88) \times 10^8$ cells/mL, respectively, due to bacterial growth in situ [Table 2; Fig. 3(b)]. The highest growth rate was obtained when the initial bacterial density was low (about 1×10^8 cells/mL); the cell density became about 2 times higher than the initial density after 2 h. When the initial bacterial density was high (about 4×10^8 cells/mL), the bacterial growth rate was about 1.5 times higher than the initial density. When the initial bacterial density was very high (about 12×10^8 cells/mL), the growth rate was about 1.25 times higher than the initial densities, which was the lowest among the three cases. The difference in bacterial growth rate might be because the relative abundance of nutrients available to the bacterial population varied depending on the initial bacterial density, with individual bacteria in more concentrated bacterial suspensions being exposed to a smaller share of the total nutrients available.

After the injection of cementation solution, about 30% of the bacteria (approximately 0.6×10^8, 2.0×10^8, and 5.2×10^8 cells/mL for the three cases) remained attached to the inner surface of the microfluidic chip compared to the number of bacteria present after bacterial settling [Table 2; Fig. 3(b)]. The actual bacterial density is expected to be higher than these values since bacterial aggregation also occurred after the cementation solution injection, especially when the bacterial density was high, and the number of bacteria present in bacterial aggregates could not be counted. The percentage of bacteria remaining (30%) is lower than that in Wang et al.

Table 2. Summary of the changes in bacterial density during MICP treatment

OD_{600} before injection	After BS injection		After settling		After CS injection	
	Average ($\times 10^8$cells per mL)	Derived ($\times 10^8$ cells per mL)	Average ($\times 10^8$cells per mL)	Derived ($\times 10^8$ cells per mL)	Average ($\times 10^8$cells per mL)	Derived ($\times 10^8$ cells per mL)
0.2	0.95867	0.03186	1.92	0.13	0.56933	0.09581
1.0	3.92333	0.28825	6.09	0.335	2.01333	0.16131
3.0	11.9	0.61644	15.4	0.875	5.212	0.78289

Note: BS = bacterial suspension; and CS = cementation solution.

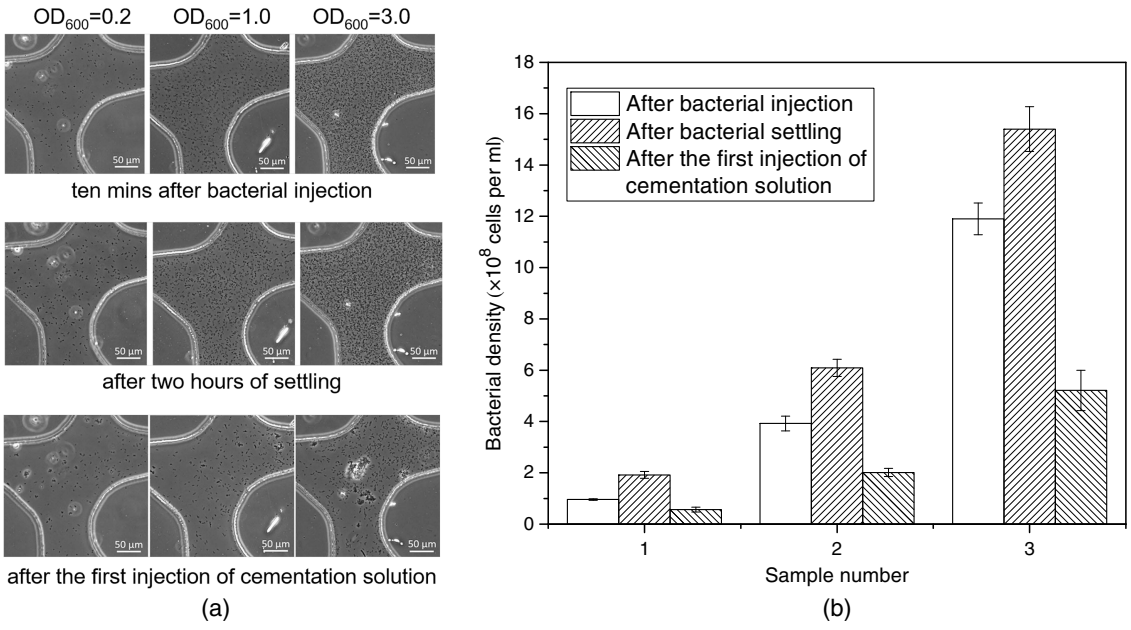

Fig. 3. (a) Microscope images of one pore at the center of the microfluidic chip containing bacterial suspensions with their initial bacterial OD_{600} were 0.2, 1.0, and 3.0, taken at 10 min after bacterial injection, after 2 h of settling and after the first injection of cementation solution; and (b) quantification of bacterial concentration in the images.

J. Geotech. Geoenviron. Eng., 2021, 147(6): 04021036

(2019a), which was 45% after the first injection of cementation solution. This might be because the bacterial settling time was 2 h in this study, which is lower than the settling time used in Wang et al. (2019a), which was 24 h. In this study, the 2 h bacterial settling time was used to study the effect of bacterial density on the kinetics and characteristics of MICP.

Bacteria's attachment to and detachment from soil particles are affected by several factors such as the surface properties of soil particles, the behavior of bacteria, and pore fluid composition (Dunne 2002; Chen et al. 2010; Liu et al. 2011; Persat et al. 2015). To simulate the surface properties of real sandy soils, the PDMS surface was treated to be hydrophilic and negatively charged and the bacterial suspension was prepared in the same condition as it could be applied in the field (Wang et al. 2019b). In addition, upscaling experiments conducted by both microfluidic chip tests and soil column tests also showed consistent results observed at both scales (Wang et al. 2020; Wang 2019). Deionized water was used to saturate the microfluidic chips in these studies, which is the same as the conditions reported in many MICP papers, but they did not consider the effects of parameters such as pH, chemicals, temperature, and dissolved oxygen of the pore fluid on the bacteria-soil interactions in real soils. The bacteria-soil interactions under the conditions that simulate real MICP-treated subsurfaces and natural environment by varying the composition of the pore fluid and environmental factors can be considered in future studies. It should be noted that there are both live and dead bacteria in the bacterial suspensions, and the current method presented in this study cannot be used to distinguish between dead and live bacterial cells. Other experimental methods are needed to investigate the effects of live and dead bacteria on the formation of calcium carbonate precipitation.

Ureolysis Rate

To examine the effect of bacterial density on the rate of ureolysis, a batch test was conducted in which the bacterial densities in bacteria-urea mixtures were varied and the hydrolysis rate was measured by using the conductivity method described by Whiffin et al. (2007). The urea concentration in the bacteria-urea mixture was 1.0 M before the hydrolysis of urea occurred (Fig. 4). Bacterial density in the range of 0.5×10^8–4×10^8 cells/mL increased the ureolysis rate (Fig. 4), while for bacterial densities exceeding around 4×10^8 cells/mL, the ureolysis rate no longer increased with bacterial density. The linear increase in ureolysis rate associated with bacterial densities in the range of 1×10^7–2×10^8 cells/mL is consistent with the results obtained by Lauchnor et al. (2015). The highest previously reported ureolysis rate was measured when bacterial density was 2×10^8 cells/mL (Stocks-Fischer et al. 1999; Lauchnor et al. 2015). However, the current study shows that when the bacterial density exceeds 5×10^8 cells/mL, the ureolysis rate does not linearly increase with bacterial density, which might be because there could be insufficient nutrients available to sustain bacterial growth at such high bacterial densities.

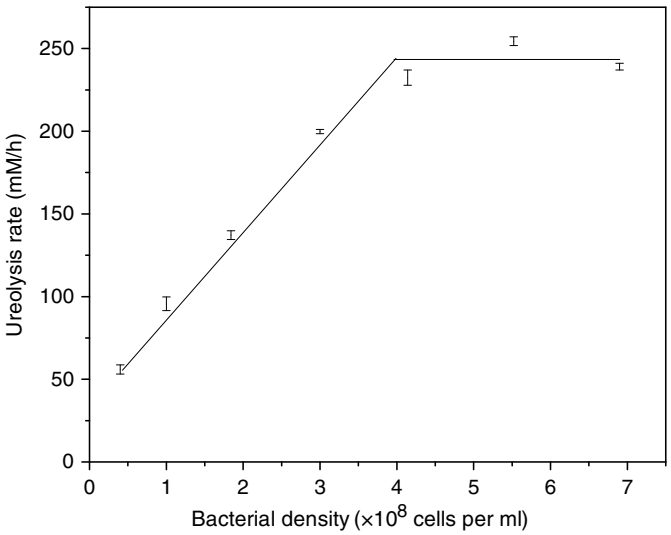

Fig. 4. Ureolysis rate plotted against bacterial density.

Bulk Precipitation Rate of $CaCO_3$

The precipitation of $CaCO_3$ with time in the three microfluidic experiments is shown in the images taken at 0.5, 1, 3, and 24 h after the cementation solution injection in Fig. 5(a). Changes in image intensity with time in the three cases with varied bacterial densities are shown in Fig. 5(b). The areas in the microfluidic chips occupied by $CaCO_3$ crystals were also different, where a higher bacterial density (e.g., 5.2×10^8 cells/mL) resulted in crystals occupying a larger area, as shown by the difference in the image intensities.

We hypothesized that the point when image intensity no longer increases indicated the completion of the $CaCO_3$ precipitation process. The time at which the image intensity stopped increasing in these three cases also varied. The time required for $CaCO_3$ precipitation to complete decreased from 15 to 1.5 h when the bacterial densities increased from 0.6×10^8 to 5.2×10^8 cells/mL. The correlation between precipitation rate and bacterial density is shown in Fig. 5(b). Bacterial density positively affects the overall $CaCO_3$ precipitation rate, and the average precipitation rates in the three cases are 0.016, 0.083, and 0.16 M/h when the corresponding bacterial densities were 0.6×10^8, 2.0×10^8, and 5.2×10^8 cells/mL, respectively.

Precipitation Rates and Sizes of Individual $CaCO_3$ Crystals

Individual $CaCO_3$ crystals are shown in the magnified images of one of the middle pores inside the microfluidic chips at 0.5, 1, 1.5, 2, 6, 15, and 24 h after the first cementation solution injection in Fig. 6(a). The average crystal volumes calculated based on the measured diameters at an interval of 15 min during the first 1.5 h and over the 24 h are plotted against time in Figs. 6(b and c), respectively. The average crystal volume data show that unlike the effect of bacterial density on the overall precipitation rate of $CaCO_3$, bacterial density does not affect the growth rate of individual $CaCO_3$ crystals. During the first 1.5 h after the injection of cementation solution, the crystals grew steadily at the same growth rate even though the bacterial density varied [Fig. 6(b)]. The crystals grew to be about 380 ± 40 μm^3 by 1.5 h for all three bacterial density cases [Fig. 6(b)].

However, the time required for the crystals to finish growing and the final size varied in the three cases. In the low bacterial density case (0.6×10^8 cells/mL case), crystal growth continued over 15 h, which was the longest among the three cases. The average size of the crystals at the completion of crystal growth was about 8,000 μm^3, which was the largest among the three cases. For the high bacterial density case (2.0×10^8 cells/mL case), the overall precipitation rate indicated that the precipitation process was completed by around 3 h [Fig. 5(b)], while individual crystal precipitation rates show that the process completed by around 10 h [Fig. 6(c)]. The growth of the crystals between 3 and 10 h is largely due to the dissolution of unstable crystals [circled in Fig. 6(a)], which contributed to the growth of larger crystals. This result is consistent with the observation obtained in Wang et al. (2019b). The final average size of the crystals was 1,800 μm^3 after 10 h. For the very high bacterial density case

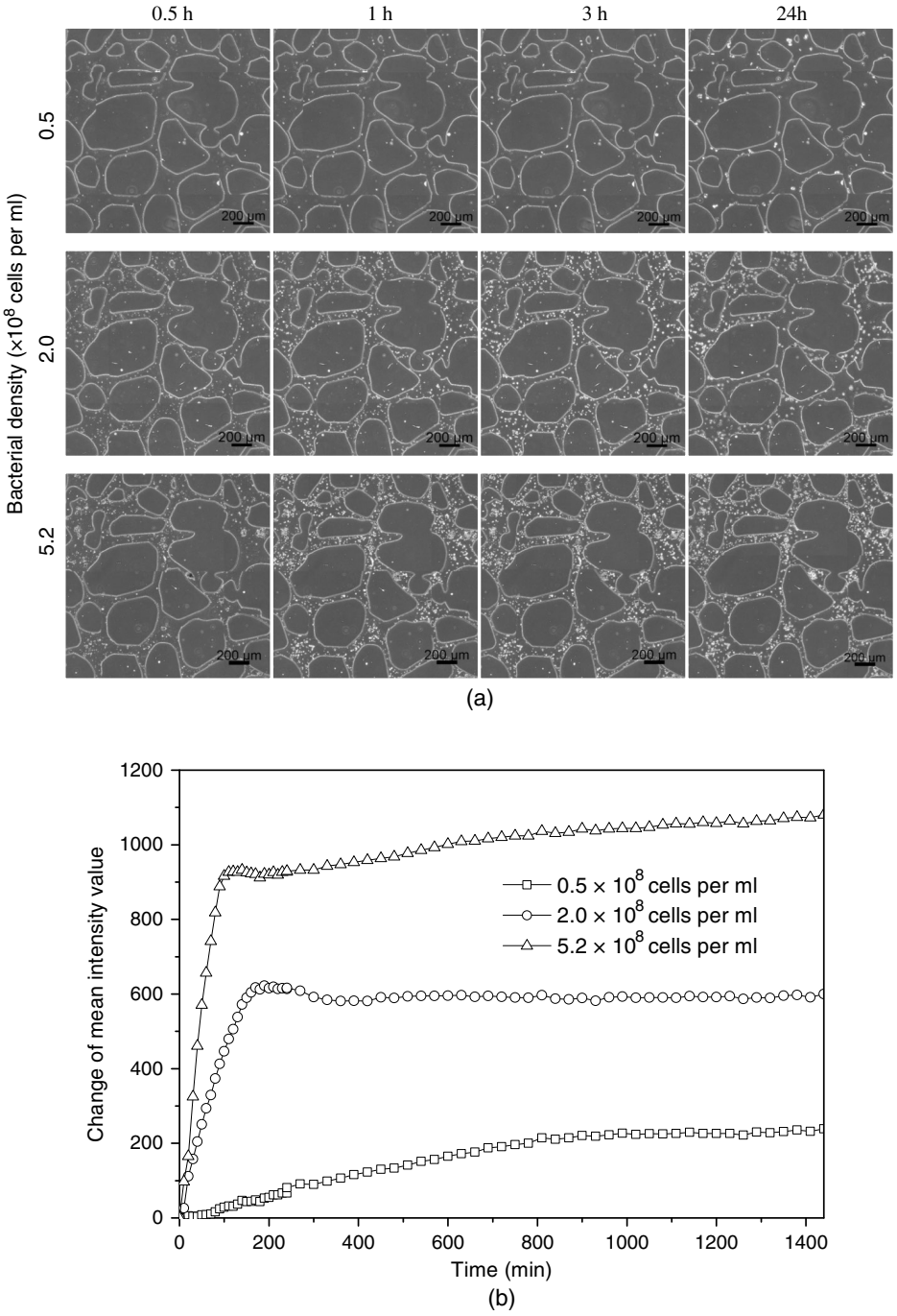

Fig. 5. (a) Microscope images taken at the center of the microfluidic chip containing bacterial suspensions at densities of 0.5, 2.0, and 5.2×10^8 cell per mL at 0.5, 1, 3, and 24 h after the first injection of cementation solution; and (b) the mean intensity value of the images versus time.

(5.2×10^8 cells/mL), crystals stopped growing by 1.5 h and the final average size of the crystals was about 400 μm^3 after 1.5 h [Figs. 6(a and b)].

Crystal Quantity

The number of crystals formed when the bacterial density was very high (5.2×10^8 cells/mL) is compared to when the bacterial density was high (2.0×10^8 cells/mL) in Figs. 5(a) and 6(a). When the bacterial density was low (0.6×10^8 cells/mL), the number of crystals was the lowest among the three cases [Figs. 5(a) and 6(a)]. To illustrate this, the number of crystals in the three cases at each instance when imaging was performed within the first 24 h was quantified (Fig. 7). The $CaCO_3$ crystal concentration represents the quantity of $CaCO_3$ crystals formed per unit volume (i.e., 1 mL). A higher bacterial density resulted in a larger quantity of crystals. When bacterial density was 0.6×10^8, 2×10^8, and 5.2×10^8 cells/mL, the concentration of crystals formed was about 1.5×10^6, 7×10^6, and 2.1×10^7 per mL, respectively, at 24 h after the cementation solution injection. Bacterial density positively correlated with the number of crystals and the overall crystal growth rate.

The change in the number of crystals with time differed among the three cases. When the bacterial density was 0.5×10^8 cells/mL, the number of crystals increased to around 2×10^6 per mL soon

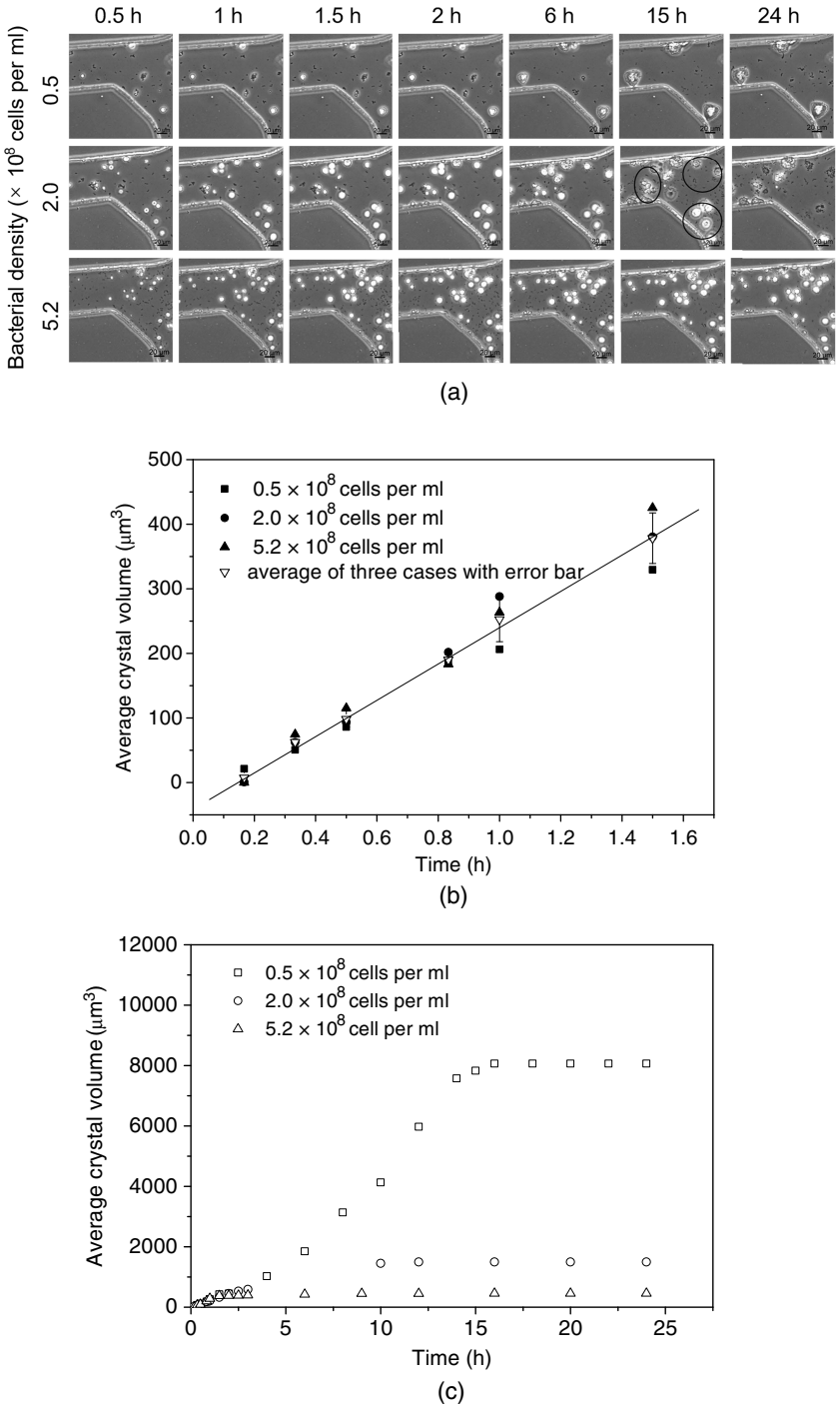

Fig. 6. (a) Microscope images taken at the center of the microfluidic chip containing bacterial suspensions at the densities of 0.5, 2.0, and 5.2×10^8 cell per mL taken at 0.5, 1, 1.5, 2.0, 6, 15, and 24 h after the first injection of cementation solution; (b) the average crystal volume versus time in the 1.5 h plotted and their liner fit; and (c) the average crystal volume versus time in the 24 h after the first injection of cementation solution.

after the cementation solution injection. When the bacterial density was 2.0×10^8 cells/mL, the number of crystals increased to around 14×10^6 per mL by 3 h and then decreased to around 7×10^6 per mL by around 10 h. The decrease in the number of crystals was due to the dissolution of unstable crystal forms. When the bacterial density was 5.2×10^8 cells/mL, the number of crystals increased to around 20×10^6 per mL by around 3 h after the cementation solution injection. Dissolution of crystals occurred but was not as obvious compared to the case when the bacterial density was 2.0×10^8 cells/mL.

Crystal Type and Dissolution

Less stable and smaller $CaCO_3$ crystals may dissolve at the expense of the growth of more stable and larger $CaCO_3$ crystals (Wang et al. 2019b). As shown in Figs. 6 and 7, crystal dissolution occurred when the bacterial density was either 2×10^8 cells/mL or 5.2×10^8 cells/mL, but not when the bacterial density was 0.6×10^8 cells/mL. To investigate the effects of bacterial density on the dissolution of the crystals, microscope images captured at different instances of each of the 12 cementation solution injections

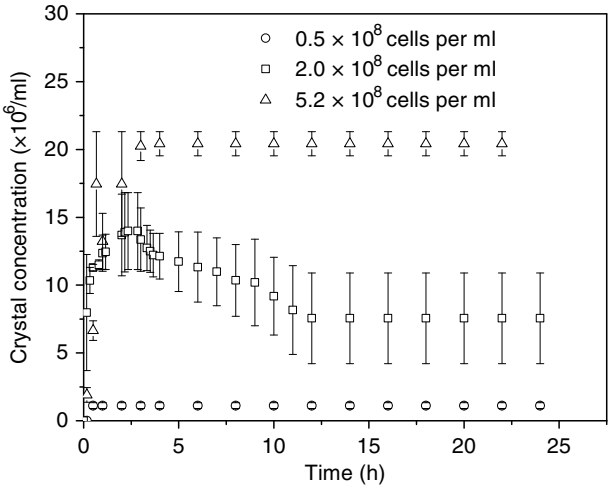

Fig. 7. Scatter plot showing the change in the concentration of $CaCO_3$ crystals with time.

are shown in Fig. 8. Figs. 8(a and b) show the images taken between 0 and 24 h after the first and the second injections of cementation solution, respectively. Fig. 8(c) shows the images taken at 24 h after the 3rd, 6th, 9th, and 12th injections of the cementation solution.

When the bacterial density was low (0.5×10^8 cells/mL in this study), the crystals that were present 24 h after the cementation solution injection were mainly prismatic, suggesting that the crystals are calcite (Al Qabany et al. 2012; Zhao et al. 2014). These crystals continued growing during the intervals between injections of cementation solution. When the bacterial density was high (2×10^8 cells/mL), the crystals that formed after injections of cementation solution were mainly spherical or prismatic. The spherical crystals were relatively unstable and often dissolved, while the prismatic crystals remained stable. Both the shape and relative solubility of these crystals are consistent with those of calcite and vaterite, respectively (Wang et al. 2019b). When the bacterial density was very high (5.2×10^8 cells/mL), bacterial aggregates were observed after the first cementation solution injection. Irregular-shaped crystals formed on top of them [Fig. 8(c)]. Spherical crystals were also observed. Although this form of $CaCO_3$ precipitates remained present after several initial injections of cementation solution [Fig. 8(c)], they were eventually replaced by more stable forms of $CaCO_3$ crystals. This suggests that when bacterial density is high, the formation of $CaCO_3$ follows the ACC-vaterite-calcite sequence, as described in Wang et al. (2019b).

A supersaturated state is required for $CaCO_3$ precipitation to occur, meaning that the solution has to contain more Ca^{2+} and CO_3^{2-} ions than could normally be dissolved by the solvent. The supersaturation ratio S has been used to quantify the level at which supersaturation induces $CaCO_3$ precipitation, which is defined as

$$S = \frac{[Ca^{2+}] \times [CO_3^{2-}]}{K_{sp}} \quad (5)$$

where $[Ca^{2+}]$ and $[CO_3^{2-}]$ = concentrations of calcium and carbonate ions; and K_{sp} = equilibrium $CaCO_3$ solubility product for each experimental temperature (Stumm and Morgan 1996). A supersaturation ratio that is higher than 1 is required for precipitation to occur.

$CaCO_3$ precipitates can exist as several polymorphs, and each has different K_{sp} values at different temperatures. At 25°C, the K_{sp} values of the four main polymorphs of $CaCO_3$ (calcite, aragonite, vaterite, and amorphous $CaCO_3$) are $10^{-8.48}$ M^2, $10^{-8.34}$ M^2, $10^{-7.91}$ M^2, and $10^{-6.40}$ M^2, respectively (Plummer and Busenberg 1982; Brečević and Nielsen 1989). Therefore, when $[Ca^{2+}] \times [CO_3^{2-}]$ is below $10^{-8.48}$ M^2, no precipitation occurs in any form; when $[Ca^{2+}] \times [CO_3^{2-}]$ is between $10^{-8.48}$ M^2 and $10^{-8.34}$ M^2, only calcite precipitates; when $[Ca^{2+}] \times [CO_3^{2-}]$ is higher than $10^{-6.40}$ M^2, all forms of $CaCO_3$ can precipitate. On the other hand, after the generation of the different forms of $CaCO_3$, when $[Ca^{2+}] \times [CO_3^{2-}]$ drops to below $10^{-6.40}$ M^2 but higher than $10^{-7.91}M^2$, amorphous calcium carbonate (ACC) dissolves, whereas the other forms of $CaCO_3$ can remain. When $[Ca^{2+}] \times [CO_3^{2-}]$ drops to between $10^{-8.48}$ M^2 and $10^{-8.34}$ M^2, all forms of $CaCO_3$ dissolve while only calcite remains. When the relatively less stable forms of $CaCO_3$ dissolve, the free Ca^{2+} and CO_3^{2-} can precipitate into the other more stable forms of $CaCO_3$ as long as the supersaturation states are reached. In addition, when multiple forms of $CaCO_3$ can precipitate at the same time, the less stable forms of $CaCO_3$ precipitate more quickly than the more stable forms of $CaCO_3$. Therefore, the ACC-vaterite-aragonite-calcite transformation may occur.

During the MICP process, Ca^{2+} ions are normally present at concentrations in the range of 0.1–1.5 M from the beginning of the $CaCO_3$ precipitation process, whereas the initial concentration of CO_3^{2-} is zero (Whiffin et al. 2007; Van Paassen 2009; Al Qabany and Soga 2013; Cheng et al. 2017). A diagram illustrating the relationship between phase transformation and the initial supersaturation state is shown in Fig. 9. The concentration of Ca^{2+} was assumed to stay constant at 1.0 M. The supersaturation state is dependent on both the hydrolysis of urea, which increases the concentration of CO_3^{2-}, and on the precipitation of $CaCO_3$, which decreases both the concentration of CO_3^{2-} and Ca^{2+}. Because bacterial density affects the bulk ureolysis rate, it also affects the supersaturation state, which in turn influences the formation of different phases of $CaCO_3$. When the bacterial density is low, the concentration of CO_3^{2-}, which is hydrolyzed from urea, increases slowly up to the calcite forming line as shown in Fig. 9, after which calcite starts forming. When the concentration of CO_3^{2-} is balanced between the forming lines of aragonite and calcite, only calcite can form. Similarly, depending on bacterial density, the other forms of $CaCO_3$ can also either form or not form, depending on whether the supersaturation state of that type of $CaCO_3$ is reached or not. When multiple forms of $CaCO_3$ precipitate, ACC-vaterite-aragonite-calcite transformation may occur.

Bacterial Aggregation and Crystal Aggregation

When the bacterial density is very high (5.2×10^8 cells/mL in this study), bacterial aggregates and crystal aggregates were observed after the first injection of the cementation solution (Fig. 8). To observe the effect of bacterial aggregates on the formation of $CaCO_3$ crystal aggregates, images of bacterial aggregates and crystal aggregates in the same spot of the microfluidic chips are shown in Fig. 10. Bacterial aggregates observed after the first injection of cementation solution are shown in Fig. 10(a). In the same spot, crystal aggregates observed after the 12th injection of cementation solution are shown in Fig. 10(b). To observe the effect of bacterial aggregates on the formation of $CaCO_3$ crystals in more detail, magnified images of the squares in Fig. 10(a) taken at 0, 20 min, 1 h, and 1 day after the first injection of cementation solution are shown in Fig. 10 (c), and the images taken 24 h after the 2nd, 3rd, 5th, and 7th injections of cementation solution are shown in Fig. 10(d).

After the first injection of cementation solution, the bacteria aggregated and irregular-shaped $CaCO_3$ crystals formed on the

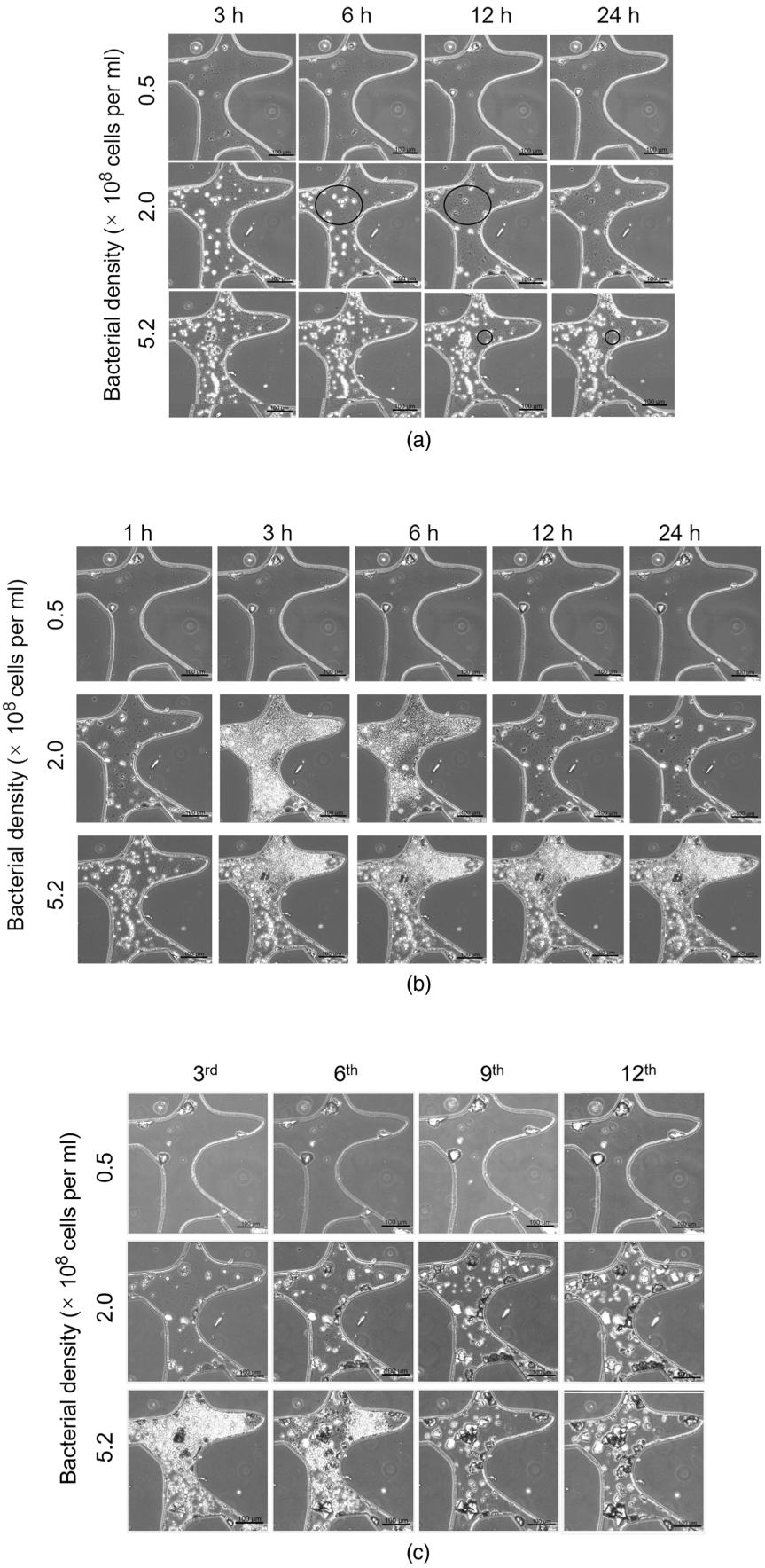

Fig. 8. Microscope images captured at (a) 3, 6, 12, and 24h after the first injection of cementation solution; (b) 0, 3, 6, and 12h, after the second injection of cementation solution; and (c) 24 h after the completion of the 3rd, 6th, 9th, and 12th injection of cementation solution.

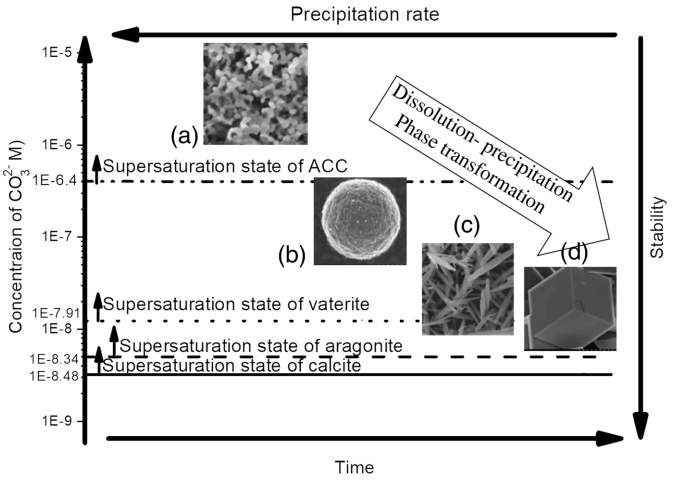

Fig. 9. Scheme illustrating the precipitation-dissolution and phase transformation of calcium carbonate (crystals), assuming the concentration of Ca^{2+} is constantly 1.0 M. [Image in (a) republished with permission of Royal Society of Chemistry, from "The kinetics and mechanisms of amorphous calcium carbonate (ACC) crystallization to calcite, via vaterite," J. D. Rodriguez-Blanco, S. Shawa, and L. G. Benning, *Nanoscale*, Vol. 3 (1), pp. 265–271, © 2011; permission conveyed through Copyright Clearance Center, Inc.; images in (b) and (d) republished with permission of Royal Society of Chemistry, from "CO_2 mineralization into different polymorphs of $CaCO_3$ using an aqueous-CO_2 system," D. H. Chu, M. Vinoba, M. Bhagiyalakshmi, I. H. Baek, S. C. Nam, Y. Yoon, S. H. Kim, and S. K. Jeong, *RSC Advances*, Vol. 3 (44), pp. 21722–21729, © 2013; permission conveyed through Copyright Clearance Center, Inc.; image in (c) Republished with permission of Royal Society of Chemistry, from "Sonochemical synthesis of aragonite-type calcium carbonate with different morphologies," G. Zhou, J. C. Yu, X. Wang, and L. Zhang, *New Journal of Chemistry*, Vol. 28 (8), pp. 1027–1031, © 2004; permission conveyed through Copyright Clearance Center, Inc.].

bacterial aggregates [Fig. 10(c), 0 min image]. The bacterial aggregates continued growing, which is shown by the increase in image intensity at 20 min compared with 0 min [Fig. 10(c), 20 min image]. At 20 min, however, spherical crystals formed on the bacterial aggregates [Fig. 10(c), 20 min image]. The spherical crystals continued growing in size during the first hour after injection [Fig. 10(c), 1 h image]. In addition, more spherical crystals also formed, but not on the bacterial aggregates [Fig. 10(c), 1 h image]. The spherical crystals were not stable, and some dissolved by 24 h after injection [Fig. 10(c), 1 day image]. During the following injections from the 2nd to the 7th, even though more unstable crystals appeared and disappeared, the crystals that were formed on the bacterial aggregates continued growing [Fig. 10(d)]. Because the crystals are so close to each other, they merged into one large crystal aggregate as they grew [Fig. 10(d), 7th injection image].

Crystal aggregates have been observed in many MICP studies (Van Paassen 2009; Cheng et al. 2017). This experiment suggests that the crystal aggregates may have formed due to crystal nucleation spots being close to each other. As the crystals grew, they merged into one big aggregate. As the number of bacteria affects the number of nucleation sites, more crystals formed when more bacterial cells were present in a given volume. Therefore, the crystals are more likely to be located closer to each other. In addition, because bacterial aggregates contain a high density of bacterial cells, the likelihood of crystals growing on or surrounding them may also be higher than the likelihood for single bacterial cells. In this particular case, the crystal aggregates present within the pores occurred at locations similar to the bacterial aggregates.

Conclusions

In this study, microfluidic chip experiments were conducted to investigate the effects of bacterial density on both the kinetics and characteristics of $CaCO_3$ precipitation at the particle scale. Three bacterial densities [0.6 (low), 2.0 (high), and 5.2×10^8 (very high) cells/mL (counted after the first cementation solution injection)] were applied in staged injection MICP procedures. Apart from bacterial density, other experimental parameters including the content and concentration of cementation solution, temperature, and injection flow rate of bacterial suspension and cementation solution were kept constant. Both the overall precipitation rate of $CaCO_3$ and the growth rate of individual $CaCO_3$ crystals were quantified. In addition, the crystal characteristics in terms of size, number, and dissolution processes were analyzed. The main findings of the study are summarized as follows.

When bacterial density is low (0.6×10^8 cells/mL in this study), the crystals form more slowly than in the higher bacterial density cases, but when sufficient time is given (15 h in this case), the sizes of $CaCO_3$ crystals were the largest among the three cases. The large crystals could be more efficient in bonding sand with larger particles and larger pore sizes. However, the number of $CaCO_3$ crystals produced is low. Improvement in terms of soil strength may require a certain amount of soil particles to be bonded by $CaCO_3$ crystals. In addition, the time required for complete $CaCO_3$ precipitation to occur is long, implying a long MICP treatment process.

When bacterial density is high (2.0×10^8 cells/mL in this study), the size of $CaCO_3$ crystals formed might be small and unstable, but over time, they may transform into larger crystals and more stable forms. The crystals formed at the particle contacts should be large enough to efficiently bond the soil particles, which in turn contributes to the strength and stiffness of MICP-treated soils. Therefore, when such a high bacterial density is used, the engineering performance efficiency of MICP-treated soils might be better when a longer treatment is applied so that the smaller crystals can reprecipitate into large ones.

When bacterial destiny is very high (5.2×10^8 cells/mL in this study), the rate of $CaCO_3$ precipitation is increased, but this may be due to the formation of large amounts of the unstable form of $CaCO_3$, ACC. The unstable forms of $CaCO_3$ undergo time-dependent transformation into more stable forms of $CaCO_3$. ACC has a lower density compared to $CaCO_3$ crystals and may be transported with the flow or trapped in soil pores. For soils that have small pores, these unstable crystals may locally clog the soil flow paths and affect the homogeneity of MICP treatment.

High bacterial density (5.2×10^8 cells/mL in this study) also contributes to the formation of bacterial aggregates after the injection of cementation solution, in turn affecting the formation of crystal aggregates. As bacterial aggregates are notably larger than individual bacteria, bacterial aggregates might be less likely to become homogenously distributed within the soil matrix, especially when they are large enough to clog the pores and prevent the transport of other bacteria and bacterial aggregates with the flow. As the formation of crystal aggregates is affected by bacterial aggregates, a nonhomogenous distribution of bacteria within a soil matrix also results in a nonhomogenous distribution of $CaCO_3$. Further work would be useful to investigate the effect of bacterial density on the distribution of bacteria and the resulting effect this has on the distribution of $CaCO_3$ content.

Based on solubility, calcite is the most stable form of $CaCO_3$ both physically and chemically, and it has been suggested that the precipitation of calcite is preferred for permanent stable cementation (Van Paassen 2009). Therefore, when designing an MICP

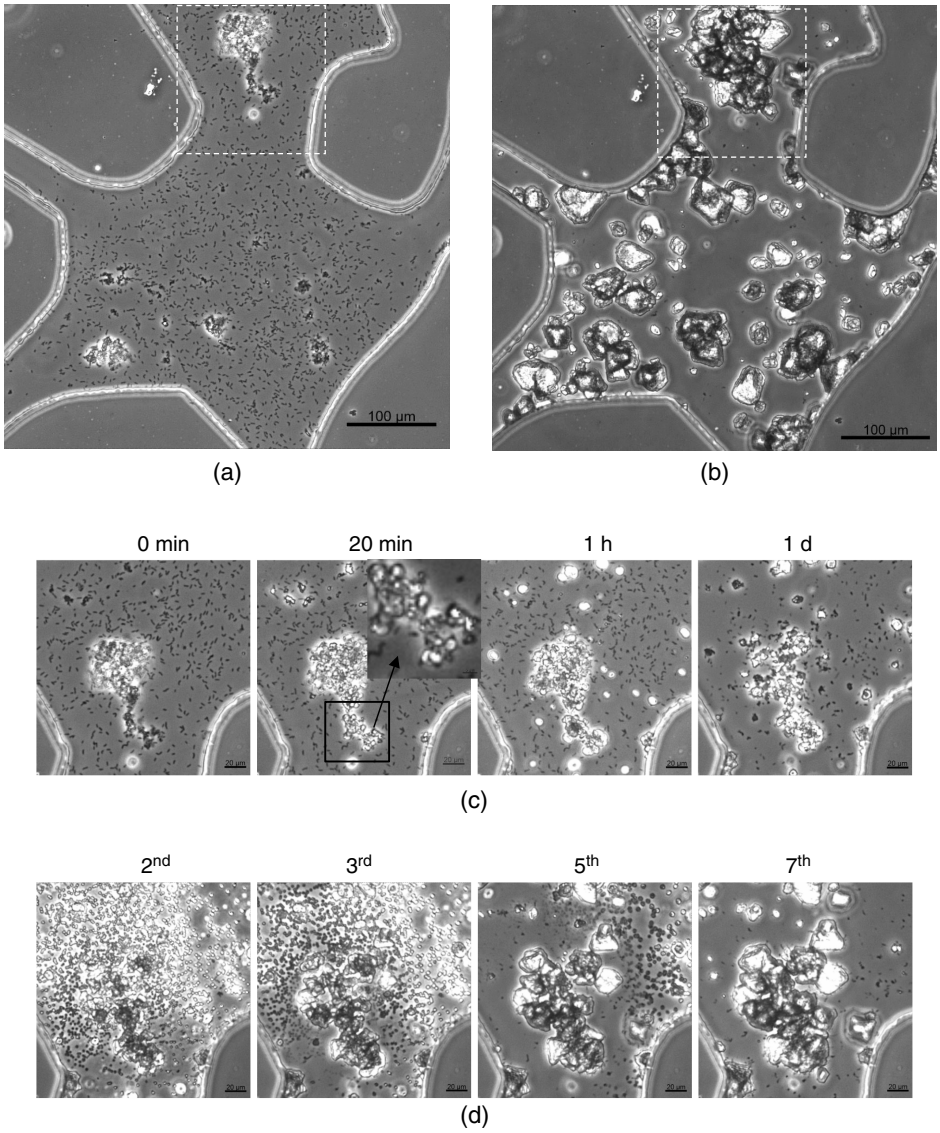

Fig. 10. (a) Bacterial aggregates formed after the first injection of cementation solution; (b) crystal aggregates formed 24 h after the 12th injection of cementation solution; (c) magnified images of the square in Fig. 10(a) taken at 0 min, 10 min, 20 min, 1h, and 1 day after the 1st injection of cementation solution; and (d) magnified images of the square in Fig. 10(a) taken at 24 h after the 2nd, 3rd, 5th, and 7th injections of cementation solution.

treatment protocol, the effects of bacterial density on the phase transformation and the time for crystals to become stable need to be considered. This study suggests that low bacterial density contributes to the production of stable $CaCO_3$ from the beginning, but the precipitation takes longer to complete. High bacterial density leads to precipitation of less stable forms of $CaCO_3$ first, even though the precipitation occurs faster. A longer treatment time is required for $CaCO_3$ to transform from less stable forms to more stable forms.

The use of microfluidic experiments is useful to assess the ideal bacterial density for various conditions in the field. MICP treatment parameters such as initial bacterial density, bacterial settling time, and injection flow rate of cementation solution all affect the delivered bacterial cell concentration in the soil matrix. Bacterial density directly affects the size and number of $CaCO_3$ crystals formed, which affect the treatment efficiency of MICP for strengthening soils. Correlations between bacterial density and the properties of $CaCO_3$ crystals in terms of number and size from this study could be helpful for the design of MICP treatment protocols for soils with different particle sizes.

Data Availability Statement

All data, models, and code generated or used during the study appear in the published article.

Acknowledgments

Y.W. would like to acknowledge Cambridge Commonwealth, European and International Trust, and China Scholarship Council, which collectively funded this project. J.T.D. acknowledges the support of the Engineering Research Center Program of the National Science Foundation under NSF Cooperative Agreement No. EEC-1449501. Any opinions, findings, and conclusions or

recommendations expressed in this manuscript are those of the authors and do not necessarily reflect the views of the National Science Foundation. The authors would like to thank Dr. David Frost of the Georgia Institute of Technology for providing the soil cross-sectional image used to design the microfluidic chip. The authors would also like to thank Dr. Fedir Kiskin for proofreading this manuscript.

References

Al Qabany, A., and K. Soga. 2013. "Effect of chemical treatment used in MICP on engineering properties of cemented soils." *Géotechnique* 63 (4): 331–339. https://doi.org/10.1680/geot.SIP13.P.022.

Al Qabany, A., K. Soga, and C. Santamarina. 2012. "Factors affecting efficiency of microbially induced calcite precipitation." *J. Geotech. Geoenviron. Eng.* 138 (8): 992–1001. https://doi.org/10.1061/(ASCE)GT.1943-5606.0000666.

Brečević, L., and A. E. Nielsen. 1989. "Solubility of amorphous calcium carbonate." *J. Cryst. Growth* 98 (3): 504–510.

Chen, G., Y. Hong, and S. L. Walker. 2010. "Colloidal and bacterial deposition: Role of gravity." *Langmuir* 26 (1): 314–319. https://doi.org/10.1021/la903089x.

Cheng, L., M. A. Shahin, and D. Mujah. 2017. "Influence of key environmental conditions on microbially induced cementation for soil stabilization." *J. Geotech. Geoenviron. Eng.* 143 (1): 04016083. https://doi.org/10.1061/(ASCE)GT.1943-5606.0001586.

Chu, D. H., M. Vinoba, M. Bhagiyalakshmi, H. Baek II, S. C. Nam, Y. Yoon, S. H. Kim, and S. K. Jeong. 2013. "CO_2 mineralization into different polymorphs of $CaCO_3$ using an aqueous-CO_2 system." *RSC Adv.* 3 (44): 21722–21729. https://doi.org/10.1039/c3ra44007a.

DeJong, J. T., M. B. Fritzges, and K. Nüsslein. 2006. "Microbially induced cementation to control sand response to undrained shear." *J. Geotech. Geoenviron. Eng.* 132 (11): 1381–1392. https://doi.org/10.1061/(ASCE)1090-0241(2006)132:11(1381).

DeJong, J. T., B. M. Mortensen, B. C. Martinez, and D. C. Nelson. 2010. "Bio-mediated soil improvement." *Ecol. Eng.* 36 (2): 197–210. https://doi.org/10.1016/j.ecoleng.2008.12.029.

DeJong, J. T., K. Soga, and E. Kavazanjian. 2013. "Biogeochemical processes and geotechnical applications: Progress, opportunities and challenges." *Géotechnique* 63 (4): 287–301. https://doi.org/10.1680/geot.SIP13.P.017.

Dunne, W. M. 2002. "Bacterial adhesion: Seen any good biofilms lately?" *Clin. Microbiol. Rev.* 15 (2): 155–166. https://doi.org/10.1128/CMR.15.2.155-166.2002.

Jiang, N.-J., K. Soga, and M. Kuo. 2017. "Microbially induced carbonate precipitation for seepage-induced internal erosion control in sand–clay mixtures." *J. Geotech. Geoenviron. Eng.* 143 (3): 04016100. https://doi.org/10.1061/(ASCE)GT.1943-5606.0001559.

Kim, D. H., N. Mahabadi, J. Jang, and L. A. van Paassen. 2020. "Assessing the kinetics and pore-scale characteristics of biological calcium carbonate precipitation in porous medium using a microfluidic chip experiment." *Water Resour. Res.* 56 (2): e2019WR025420. https://doi.org/10.1029/2019WR025420.

Lauchnor, E. G., D. M. Topp, A. E. Parker, and R. Gerlach. 2015. "Whole cell kinetics of ureolysis by Sporosarcina pasteurii." *J. Appl. Microbiol.* 118 (6): 1321–1332. https://doi.org/10.1111/jam.12804.

Liu, J., R. M. Ford, and J. A. Smith. 2011. "Idling time of motile bacteria contributes to retardation and dispersion in sand porous medium." *Environ. Sci. Technol.* 45 (9): 3945–3951. https://doi.org/10.1021/es104041t.

Martinez, B. C., J. T. DeJong, T. R. Ginn, B. M. Montoya, T. H. Barkouki, C. Hunt, and D. Major. 2013. "Experimental optimization of microbial-induced carbonate precipitation for soil improvement." *J. Geotech. Geoenviron. Eng.* 139 (4): 587–598. https://doi.org/10.1061/(ASCE)GT.1943-5606.0000787.

Montoya, B., J. DeJong, and R. Boulanger. 2013. "Dynamic response of liquefiable sand improved by microbial-induced calcite precipitation." *Géotechnique* 63 (4): 302–312. https://doi.org/10.1680/geot.SIP13.P.019.

Persat, A., C. D. Nadell, M. K. Kim, F. Ingremeau, A. Siryaporn, K. Drescher, and H. A. Stone. 2015. "The mechanical world of bacteria." *Cell* 161 (5): 988–997. https://doi.org/10.1016/j.cell.2015.05.005.

Plummer, L. N., and G. E. Busenberg. 1982. "The solubilities of calcite, aragonite and vaterite in CO_2-H_2O solutions between 0 and 90°C and an evaluation of the aqueous model for the system $CaCO_3$-CO_2-H_2O." *Geochim. Cosmochim. Acta* 46 (6): 1011–1040. https://doi.org/10.1016/0016-7037(82)90056-4.

Rodriguez-Blanco, J. D., S. Shaw, and L. G. Benning. 2011. "The kinetics and mechanisms of amorphous calcium carbonate (ACC) crystallization to calcite, via vaterite." *Nanoscale* 3 (1): 265–271. https://doi.org/10.1039/C0NR00589D.

Stocks-Fischer, S., J. K. Galinat, and S. S. Bang. 1999. "Microbiological precipitation of $CaCO_3$." *Soil Biol. Biochem.* 31 (11): 1563–1571. https://doi.org/10.1016/S0038-0717(99)00082-6.

Stumm, W., and J. J. Morgan. 1996. *Aquatic chemistry.* 3rd ed. New York: Wiley.

Van Paassen, L. 2009. "Biogrout: Ground improvement by microbially induced carbonate precipitation." Ph.D. thesis, Dept. of Biotechnology, Delft Univ. of Technology.

Wang, Y. 2019. "Microbial-induced carbonate precipitation (MICP) from micro to macro scales." Ph.D. thesis, Dept. of Engineering, Univ. of Cambridge.

Wang, Y., C. Konstantinou, K. Soga, J. T. DeJong, G. Biscontin, and A. J. Kabla. 2020. "Enhancing strength of MICP-treated sandy soils: From micro to macro scale." Preprint, submitted June 29, 2020. http://arxiv.org/abs/2006.15760.

Wang, Y., K. Soga, J. DeJong, and A. Kabla. 2019a. "A microfluidic chip and its use in characterizing the particle-scale behaviour of Microbial-Induced Carbonate Precipitation (MICP)." *Géotechnique* 69 (12): 1086–1094. https://doi.org/10.1680/jgeot.18.P.031.

Wang, Y., K. Soga, J. DeJong, and A. Kabla. 2019b. "Microscale visualization of microbial-induced carbonate precipitation (MICP) processes." *J. Geotech. Geoenviron. Eng.* 145 (9). https://doi.org/10.1061/(ASCE)GT.1943-5606.0002079.

Wang, Y., K. Soga, and N.-J. Jiang. 2017. "Microbial induced carbonate precipitation (MICP): The case for microscale perspective." In *Proc., 19th Int. Conf. on Soil Mechanics and Geotechnical Engineering*, 1099–1102. Cambridge, UK: University of Cambridge.

Whiffin, V. S., L. A. van Paassen, and M. P. Harkes. 2007. "Microbial carbonate precipitation as a soil improvement technique." *Geomicrobiol. J.* 24 (5): 417–423. https://doi.org/10.1080/01490450701436505.

Zapata, A., and S. Ramirez-Arcos. 2015. "A comparative study of McFarland turbidity standards and the densimat photometer to determine bacterial cell density." *Curr. Microbiol.* 70 (6): 907–909. https://doi.org/10.1007/s00284-015-0801-2.

Zhang, W., Y. Ju, Y. Zong, H. Qi, and K. Zhao. 2018. "In situ real-time study on dynamics of microbially induced calcium carbonate precipitation at a single-cell level." *Environ. Sci. Technol.* 52 (16): 9266–9276. https://doi.org/10.1021/acs.est.8b02660.

Zhao, Q., L. Li, C. Li, M. Li, F. Amini, and H. Zhang. 2014. "Factors affecting improvement of engineering properties of MICP-treated soil catalyzed by bacteria and urease." *J. Mater. Civ. Eng.* 26 (12): 04014094. https://doi.org/10.1061/(ASCE)MT.1943-5533.0001013.

Zhou, G. T., C. Y. Jimmy, X. C. Wang, and L. Z. Zhang. 2004. "Sonochemical synthesis of aragonite-type calcium carbonate with different morphologies." *New J. Chem.* 28 (8): 1027–1031. https://doi.org/10.1039/b315198k.